



RESEARCH ARTICLE

Electromechanical ice protection system: de-icing capability prediction considering impedance matching effect

B. Miao¹, L. Yuan¹ and C.L. Zhu²

¹College of Aerospace Engineering, Nanjing University of Aeronautics and Astronautics, Nanjing, Jiangsu, China and ²State Key Laboratory of Mechanics and Control of Mechanical Structures, Nanjing University of Aeronautics and Astronautics, Nanjing, Jiangsu, China

Corresponding author: C.L. Zhu; Email: clzhu@nuaa.edu.cn

Received: 26 September 2023; **Revised:** 2 February 2024; **Accepted:** 5 February 2024

Keywords: Electromechanical de-icing system; De-icing capability; Impedance-matching; Piezoelectric actuator; Mechanical vibration

Abstract

Due to the safety threats caused by icing, the de-icing system is essential in the aviation industry. As an effective method, the electromechanical de-icing system (EDS) is a new ice-protection system based on mechanical vibration principles. For the majority of the current research on system de-icing capability estimation, the effect of impedance-matching is not considered. Impedance matching plays a very important role in improving the performance of the electromechanical system, so we must also consider the impact of impedance matching when designing the EDS. In the present study, a de-icing capability prediction method considering the impact of an impedance-matching device is established based on experimental and numerical methods. The results indicate that the impedance-matching effect has no impact on the mechanical vibration of the structure for the same load power. Meanwhile, impedance-matching devices can significantly improve the power factor and increase the interface shear stress/strain for de-icing. Eight different vibrational modes were tested, and the experimental results showed that the actual interface shear strain after impedance matching is inversely proportional to the de-icing time. The verification experiments were conducted and the accuracy of the proposed prediction method was verified.

Nomenclature

a, b	length and width of the plate, m
A	integration coefficient
E, μ	Young's modulus and Poisson's ratio of the structure
F_{stru}	motivating force applied to the structure
h_{alu}, h_n	plate thickness and the position of the neutral line, m
m, n	number of anti-nodes in the transversal and longitudinal axes
\bar{M}, D, \bar{K}	mass matrix, damping matrix, and stiffness matrix
$P_{sys, i}$	power of the vibration mode i
q_i	displacement
$Q_{m, i}$	quality factor of the vibration mode
$v_{vel, i}$	velocity of the vibration mode i , m/s
w	displacement in x-, y-, and z-directions, m
σ, ε	main stress and strain, Pa
τ, γ	shear stress and strain, Pa
θ	angle between equivalent resistance and equivalent reactance
ε_{damp}	damping ratio
ρ	density, kg/m ³

1.0 Introduction

The icing of aircraft and wind turbines causes component damage, results in operation disruption, and inherent equipment loss, as well as their potential for causing serious accidents [1, 2]. Different types of anti/de-icing methods, such as thermal [3], mechanical [4], chemical [5] and other methods with new principles guide (for example, plasma [6]) have been introduced by researchers to deal with the ice threat. With high reliability and efficiency, ice-protection systems are commonly used on aviation equipment with thermology methods [3]. Superhydrophobic-coating and plasma-ice-protection methods have become research hot topics in recent years because of the rapid development of emerging materials and active control technology [7, 8]. In smart-materials applications and their related smart-actuator applications [9], new electromechanical de-icing technologies, which are energy-saving, nonthermal and low-weight, and meet green-energy transportation needs, have existed since 1998 [10], developing rapidly after 2016 [11, 12].

Electromechanical ice-protection technology is a mechanical technology and the vibration sources of this method come from piezoelectric actuators. The above-mentioned technology uses structural vibration or ultrasonic waves to induce shear stress at the interface of the ice/substrate and to destroy the adhesion between the two components. Based on this ice-removal principle, electromechanical resonant de-icing has been widely studied. Venna et al. studied the vibration characteristics of leading-edge structures with piezoelectric actuators in the simulation method and conducted the de-icing experiment in a cold environment to reveal the advantages of low-energy consumption [13]. Investigation of an ultrasonic ice protection system with piezoelectric actuators on helicopter rotor blades was presented by Palacios et al. and instantaneous ice delamination was obtained during the experiments [14, 15]. Electromechanical de-icing researches with different vibration modes, as well as the related relationships between ice removal and vibration modes, were also been studied by Budinger et al. in the aspect of resonant vibration [16] and Guo et al. in the point view of ultrasonic guide waves [17]. Moreover, feasibility research of the electromechanical de-icing technology on glass fiber-reinforced composite materials was also conducted by many scholars in the development of wind energy equipment [18–20]. In addition to the above research status about the electromechanical de-icing method, some special items relating to this method also be investigated based on different application considerations. Daniliuk et al. [21], Wang et al. [22] and Shi et al. [23] discussed the importance of ultrasonic transducers in the electromechanical de-icing method and introduced different de-icing application results of various types of piezoelectric-based transducers. Overmeyer et al. and Miao et al. considered the impact of the adhesive layer on the final de-icing results [24, 25]. Combining the application of the electromechanical de-icing method with other de-icing technologies (such as the electrothermal method or ice-phobic coating) has also been investigated by some researchers to improve the de-icing efficiency [26–28].

In ultrasonic electromechanical de-icing technology, the sufficient output power to excite the overall structure vibration is the critical aspect to be considered for de-icing system design. As with the widely used electrothermal de-icing method, the transfer of electric heat energy from the heating elements to the substrate is a crucial aspect to be considered during the de-icing process. Therefore, for the mechanical vibration de-icing method, the transfer of energy from the excitation source to the structure to increase the vibration amplitude for efficient de-icing must be given the highest priority. In the field of ultrasonic transducers, researchers have developed various methods to enhance the energy transfer efficiency of piezoelectric transducers and ensure minimal power loss during operation, based on specific objectives [29–31]. The impedance-matching circuit is found to be the main component for conducting the impedance-matching operation. This circuit has two functions: 1) transform the impedance of the ultrasonic device into the impedance value required by the ultrasonic signal excitation source, and 2) use inductive components to compensate for the capacitive impedance of the ultrasonic device, to improve the output power of the whole system [30]. The addition of inductive components to the original driving system is a common method used in the practical application of many ultrasonic transducers. This second function of the circuit is favoured due to its ease of adjustment [30, 31].

The impedance considerations during EDS design were found in some works of literature. The common way to deal with the impedance issue during the EDS operating period is to find the specific frequency with the lowest impedance values by using the impedance analyser [11]. The majority of the studies on the design of EDS use this approach. Palacios et al. highlighted the method to find the driving mode according to the impedance characteristics of the actuator when conducting the de-icing tests in the ice wind tunnel [11]. Leandro et al. [32] also used the impedance magnitude curve to determine the final exciting frequency of actuators. For the relationship between impedance and natural frequencies of structures, the inflection point of the impedance variation curve represents the natural frequency value of each order. So the resonant vibration of EDS was introduced by many scholars to design the target de-icing frequencies according to different natural vibration modes [11, 13–16]. Budinger et al. [33] analysed the fracture propagation mechanisms of the ice layer under the excitation of an electromechanical resonant de-icing system with different resonant vibration mode types (flexural modes and extensional modes). Villeneuve et al. designed the piezoelectric de-icing system according to some typical natural vibration modes and achieved ice delamination on flat plate and wing structures [34]. Apart from this research on impedance considerations, only Leandro et al. introduced an adaptive impedance matching network into EDS to improve the output power [35]. The network was included with several electrical components of capacitors and inductances. And the adjustment of these components was according to the impedance measurement data. The voltage under the matched network had a percentage increase of about 102% than the voltage with an unmatched situation.

As described earlier, the influence of impedance is important for the designing of EDS. Meanwhile, impedance is a typical power-influencing factor in the system with electromechanical transducers. According to the current state of impedance considerations in EDS design, most researchers have only used passive means to determine the excitation frequency and ensure the minimum impedance value. This method cannot meet the requirement of precise modal control and transformation during the de-icing process. After analysing the research on impedance matching circuits and drawing inspiration from the findings of Leandro et al, the implementation of an active impedance control strategy in the design process of EDS proves to be an effective approach to improving de-icing performance and efficiency. The effects of impedance matching are tested by employing specific experiments. The means of prediction by simulation calculations are relatively lacking. There is also a lack of studies that consider the effect of impedance matching on the shear stress during de-icing excitation. For the design of EDS, it is a priority to find an evaluation method that can easily examine the de-icing performance of EDS integrated with impedance-matching devices under different vibration modes.

To achieve the above research objectives, this paper is governed as the following sections. Firstly, the introduction is presented in section 2.0 for the basic theory for establishing the de-icing capability prediction method of the de-icing system with the influence of an impedance-matching device. Detailed descriptions of the simulation model using finite element analysis software and relative experiment setups used in this paper are also given in section 2.0. The simulation model is validated by experiment data in the aspect of mechanical and electrical characteristics. Section 3.0 discusses the influence of impedance matching devices on the power and vibration characteristics of the de-icing system, as well as the verification of the established prediction method. The detailed de-icing tests of EDS integrated with impedance-matching devices under different vibration modes are also presented and discussed in section 3.0.

2.0 Models and methods

2.1 Description of the de-icing capability prediction method

Structures in aviation equipment are always thin-walled structures, especially the aerofoil wings. So the basic theories of vibration with piezoelectric actuators were established based on thin-walled structure. For the model we used in this research is the electromechanical coupled structure, which includes the aluminum plate and piezoelectric actuators. The vibrational characteristics and stress/strain features on

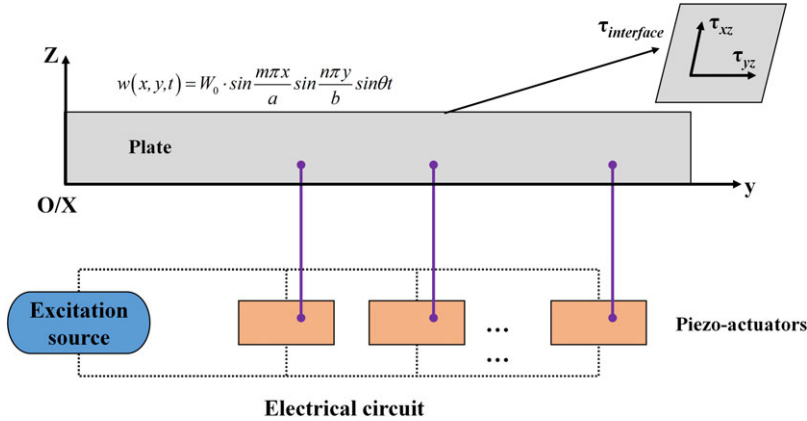


Figure 1. Frame diagram of the research model.

the aluminum plate are the main factors to induce the delamination of ice. So in this research, we adopt the model introduced by Budinger et.al, and provided the detail description of the de-icing capability prediction method. For better presentation of the research model and problem, a schematic to describe the research model was added in the manuscript, which was shown in Fig. 1.

If we assume the z-displacement as the following expression in Equation (1) for a thin plate and use the model introduced by Budinger [16, 36, 37], the interface shear stress/strain is given by Equation (2).

$$w(x, y, t) = W_0 \cdot \sin \frac{m\pi x}{a} \sin \frac{n\pi y}{b} \sin \theta t \tag{1}$$

$$\begin{aligned} \tau_{inter-shear} &= \sqrt{\tau_{xz}^2 + \tau_{yz}^2} = A \cdot W_0 \\ &= \frac{E}{1 - \mu^2} \cdot W_0 \cdot \sin \theta t \left[\left(\frac{m\pi}{a} \right)^2 + \left(\frac{n\pi}{b} \right)^2 \right] \frac{(h_{alu} - h_n)^2 - h_n^2}{2} \dots \\ &\dots \sqrt{\left(\frac{m\pi}{a} \right)^2 \cos^2 \frac{m\pi x}{a} \sin^2 \frac{n\pi y}{b} + \left(\frac{n\pi}{b} \right)^2 \sin^2 \frac{m\pi x}{a} \cos^2 \frac{n\pi y}{b}} \end{aligned} \tag{2}$$

Where m and n are the numbers of anti-nodes in the transversal and longitudinal axes, respectively; a and b are the length and width of the plate, respectively; h_{alu} and h_n are the plate thickness and the position of the neutral line, respectively; and A is an integration coefficient.

The mechanical power of a mechanical vibration structure can be defined as a function of force and velocity. We can thus evaluate the vibrational power of the structure as follows:

$$P_{sys} = \frac{1}{2} \cdot F_{stru} \cdot v_{vel} \tag{3}$$

Where F_{stru} is the motivating force of the structure, which has the following expression in the case of the relative electromechanical parameters of the whole system:

$$F_{stru,i} = N_i V_{elec,i} = j D_s \omega_i q_i = j \frac{\sqrt{K_i M_i}}{Q_{m,i}} \omega_i q_i = j \frac{M_i \omega_i^2}{Q_{m,i}} q_i \tag{4}$$

Where D_s is the damping coefficient and $Q_{m,i} = 1/2\varepsilon_{damp}$ is the quality factor of the vibration mode.

Deriving the simultaneous equations, Equations (2)–(4) yield the following relationships between power, peak displacement, and interface shear stress/strain. The following equation shows that interface shear stress/strain is proportional to the displacement and proportional to the square root of the power.

$$\begin{aligned}
 P_{sys,i} &= \frac{1}{2} \cdot F_{stru,i} \cdot v_{vel,i} = \frac{1}{2} \cdot \frac{M_i \omega_i^2}{Q_{m,i}} q_i \cdot \dot{q}_i = \frac{1}{2} \cdot \frac{M_i \omega_i^3}{Q_{m,i}} q_i^2 \\
 &= \frac{1}{2} \cdot \frac{M_i \omega_i^3}{Q_{m,i}} W_{0,i}^2 = \frac{1}{2} \cdot \frac{M_i \omega_i^3}{Q_{m,i}} A_i^{-2} \tau_{inter-shear,i}^2
 \end{aligned}
 \tag{5}$$

$$ISCC = \frac{\tau_{inter-shear,i}}{\sqrt{P_{sys,i}}} = A_i \sqrt{\frac{2Q_{m,i}}{M_i \omega_i^3}}
 \tag{6}$$

Equation (5) shows that the rate between interface shear stress/strain and power will yield a constant for a specific excitation frequency, which is shown in Equation (6). The rate was presented firstly by Palacios et al. [14, 15] in the de-icing technology study with ultrasonic guide waves and defined as Interface Stress Concentration Coefficient (ISCC). This coefficient was established under the excitation of ultrasonic guide waves and only focused on the structure with plate and actuators.

According to the basic principles of the mechanical vibration-ice-protection method, interface shear stress/strain is the main cause of ice delamination [12]. In ultrasonic equipment, load power and output power are always treated as the main parameters for output ability evaluation [21, 37]. Furthermore, output power or its related parameters (such as driving voltage and current) are all direct parameters to be controlled when carrying out ice-protection experiments. Many scholars tried to improve the output power of actuators using different impedance-matching methods to enhance the de-icing efficiency. So, predicting the de-icing capability considering the impedance matching effect is very necessary for the actual ice protection application.

The ISCC was derived without considering the impedance-matching effect. The ISCC can only be obtained by simulation or experiment method without regard to the impact of impedance-matching. The influence of impedance matching cannot be considered in the simulation calculation. Regarding the effect of impedance-matching, there is a gap between simulation calculation and practical application. Therefore, establishing a prediction method to judge the de-icing capability of specific vibration modes considering the impedance-matching effect through a special method is the important target to be researched in this paper.

On the basis of the expression in Equation (5), the existence of a series matching inductor is an electrical component, not a mechanical device. It was assumed that the ISCC value for a given vibrational mode would not be affected by the presence of an impedance matching device. Observing the relationship between shear stress/strain and power, when the improved power $P_{actual,i}$ of the system can be obtained by adding the series-matching inductor, the corresponding interface shear stress/strain can be predicted by the following equation:

$$\begin{aligned}
 \tau_{actual,i} &= \frac{\tau_{inter-shear,i}}{\sqrt{P_{sys,i}}} \cdot \sqrt{P_{actual,i}} = ISCC_\tau \cdot \sqrt{P_{actual,i}} \\
 \gamma_{actual,i} &= \frac{\gamma_{inter-shear,i}}{\sqrt{P_{sys,i}}} \cdot \sqrt{P_{actual,i}} = ISCC_\gamma \cdot \sqrt{P_{actual,i}}
 \end{aligned}
 \tag{7}$$

So the values of ISCC for a specific vibration frequency will be a constant, whether it is obtained by simulation or experimental test. Due to the difficulty of considering the impedance-matching effect in simulation calculation, from the perspective of practical de-icing applications, the proposed method for predicting de-icing capability with impedance-matching can be summarised and given in the following application procedure:

- (1) ISCC value at one specific vibration frequency is calculated through the simulation method without considering impedance matching devices (with Equation (6)).
- (2) The de-icing system is connected with the impedance matching devices for actual pre-excitation vibration testing to record the actual load power.

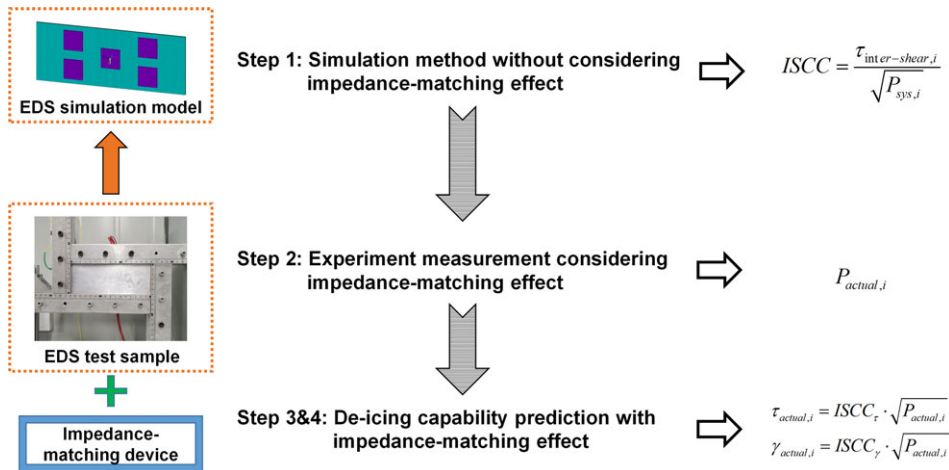


Figure 2. Frame diagram of the de-icing capability prediction method.

- (3) Actual interface shear stress/strain at one specific vibration frequency is predicted based on the measured power and the expression of Equation (7).
- (4) De-icing capability at one specific vibration frequency is predicted according to the magnitude of the actual interface shear stress/strain.

The frame diagram of the de-icing capability prediction method can be summarised as the following architecture shown in Fig. 2. If the ISCC value is determined by the simulation method, the interface shear stress/strain in other situations under different input power will be predicted according to this value. Meanwhile, this method is particularly suitable for the prediction of interfacial shear stress/strain in cases where the structure has an ice layer attached.

For the de-icing capability prediction method established in this paper, although the two types of typical parameters (interface shear stress/strain and power) were derived from theoretical derivations, they could also be used in other related DES models through simulation and experimental method. So the prediction method introduced in the paper can be used in the actual application.

2.2 Simulation model settings

An aluminum plate with five piezoelectric patches was selected as the substrate for the simulation. The dimensions of the plate and the piezoelectric actuators were 160 mm × 60 mm × 2 mm and 20 mm × 20 mm × 1.5 mm, respectively. The actuator material was PZT-8. Detail simulation processes were conducted by the commercial finite element simulation software ANSYS®. According to our previous results about the verification of mesh independence, a mesh size of 0.001 m was set as the basic grid length for the whole system modeling [25]. For the actual wing skin surface on the aircraft, the wing skin was attached on the wing foundation structures (such as rib structure) with rivets. So the boundary conditions of the wing skin surface were clamped conditions. That's the reason why clamped conditions were applied on the four edges of the plate. Five piezoelectric actuators were bonded onto one surface of the plate. The plate was modeled with the 8-node quadrilateral element Solid 185 for solid materials. The 8-node quadrilateral element Solid 5 (for coupling situations) was chosen to model the piezoelectric actuators. The material information of the aluminum and PZT-8 is listed in Table 1. The voltage single were applied onto the surface of piezoelectric according to the detail simulation requirement. Vibrational mode shapes shown in the results were obtained by modal analysis, while detail vibrational results in mechanical aspect and electrical aspects were obtained by harmonic response analysis.

Table 1. Material parameters of PZT-8 and aluminum

Material	Density ($\text{kg}\cdot\text{m}^{-3}$)	Young's modulus (GPa)	Poisson's ratio	Dielectric constant ($\times 10^{-9}$) ($\text{F}\cdot\text{m}^{-1}$)	Elasticity coefficient ($\times 10^{10}$) ($\text{N}\cdot\text{m}^{-2}$)	Piezoelectric coefficient ($\text{C}\cdot\text{m}^{-2}$)
Aluminum	2780	70.5	0.33	–	–	–
PZT-8	7600	–	–	$\begin{bmatrix} 7.9688 & 0 & 0 \\ 0 & 7.9688 & 0 \\ 0 & 0 & 5.3125 \end{bmatrix}$	$\begin{bmatrix} 14.9 & 8.11 & 8.11 & 0 & 0 & 0 \\ 0 & 14.9 & 8.11 & 0 & 0 & 0 \\ 0 & 0 & 13.2 & 0 & 0 & 0 \\ 0 & 0 & 0 & 3.13 & 0 & 0 \\ 0 & 0 & 0 & 0 & 3.13 & 0 \\ 0 & 0 & 0 & 0 & 0 & 3.4 \end{bmatrix}$	$\begin{bmatrix} 0 & 0 & -4.1 \\ 0 & 0 & -4.1 \\ 0 & 0 & 14 \\ 0 & 10.3 & 0 \\ 10.3 & 0 & 0 \\ 0 & 0 & 0 \end{bmatrix}$

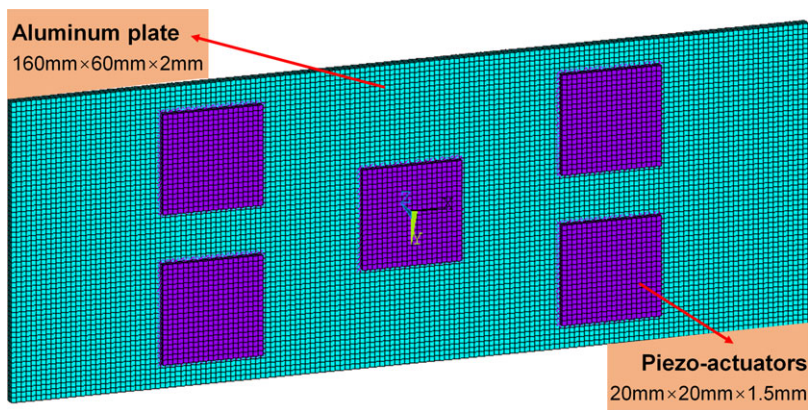


Figure 3. Schematic diagram of the simulation model.

A schematic diagram of the simulation model is shown in Fig. 3. Because of the unpredictable icing situation and random icing size in real applications, no ice layer was included in the model. Therefore, coupled structures, containing aluminum plates and piezoelectric actuators, were treated as a new electromechanical actuator component for detailed study in this paper. Unpredictable ice components were considered as the load for this new type of electromechanical actuator. The uncertain factors related to icing can be eliminated in the careful design of the ice-protection structure. Therefore, the plate, in this paper, constituted the main working surface of the overall de-icing actuators. De-icing mode selection was evaluated on the upper surface of the plate, while electromechanical features were evaluated from the perspective of the overall electromechanical actuator component. The aim of this research work introduced in this text was to establish a feasible method for predicting the de-icing capability taking into account the impedance matching effect. This method can be applied to ultrasonic de-icing structures with any piezoelectric actuator layout scheme. Therefore, we adopted the same piezoelectric actuator layout without considering the influence of the location and quantity of the specific piezoelectric actuators.

2.3 Experimental setups

Figure 4 shows detailed information on the main substrate for ice protection. The dimensions of the plate and the arrangement of piezoelectric actuators were consistent with the simulation model settings. The piezo-actuators array used in this research was not carefully designed but merely ensured the symmetry of the distribution. The de-icing structure was fixed by jigs manufactured by aluminum profiles. Meanwhile, scale markings were attached to the support structure near the four edges of the plate for the aim of subsequent positioning of the points on the plate. The experiments are performed on a clamped plate. As introduced in the above paragraph, the clamped boundary conditions of the plate were determined according to the actual attachment situation of wing skin on the aircraft. So the research objects used in simulation and experimental studies were contextualised to the actual application.

The experimental setups in this paper were divided into three different systems with various testing aims: (1) a system for structural-vibration characteristics measurement; (2) a system for electrical-parameter measurement of the coupled electromechanical de-icing structure; and (3) a system for ice-removal testing and observation. The corresponding schematic diagrams of these experimental setups are shown in Fig. 5. The mechanical vibrational characteristics and the electromechanical features were all tested to provide information for further study. Firstly, the setup for the vibrational model-shapes measurement was carried out by a PSV-500-3D scanning laser vibrometer, which was shown in Fig. 4a. Relative vibration response of the de-icing structure can also be obtained by this setup. The electrical parameters of the whole de-icing system were calibrated using a Microtest-6632 precision-impedance

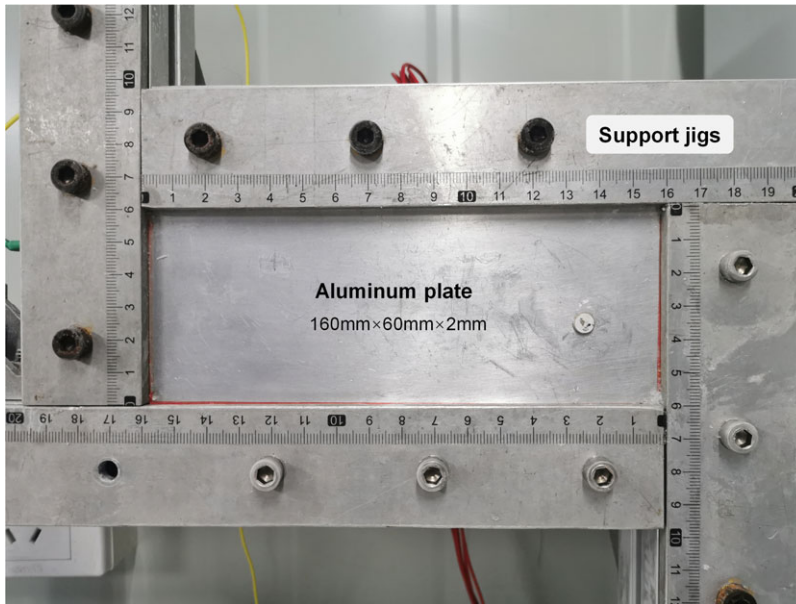


Figure 4. Detailed information on the main substrate for ice protection.

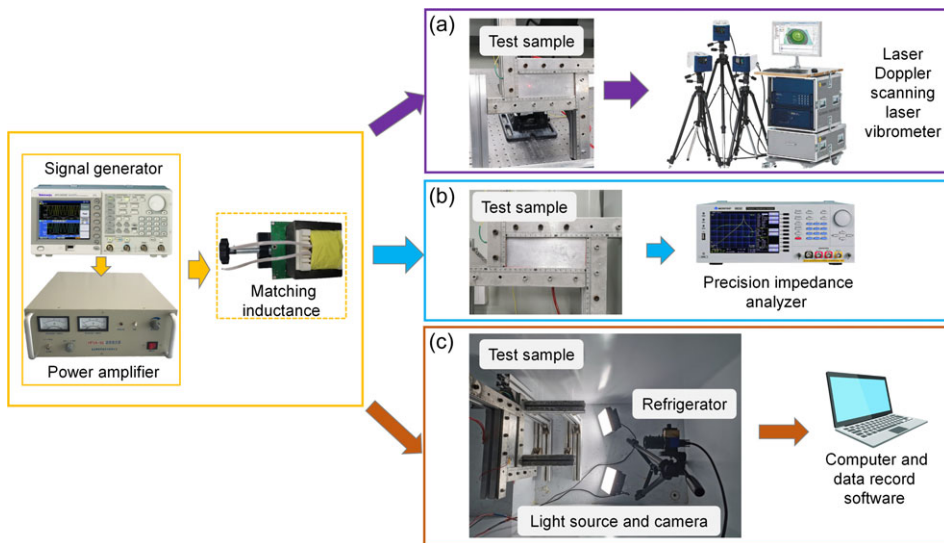


Figure 5. Experiment setups for actual data measurement and de-icing testing.

analyser, the schematic of this setup was shown in Fig. 4b. Meanwhile, the vibration response of structures under the influence of impedance matching device could be measured by combing the setups in Fig. 5a and 5b together. The vibration displacement for specific positions was tested by the SOPTOP LV-S01 single-point laser vibrometer. Figure 5c shows the de-icing structure and system. The cold environment was guaranteed by a refrigerator with a constant low-temperature retention function. A low-temperature industrial camera and its corresponding light source were used to record the ice removal in the refrigerator. The actual videos during de-icing experiments can be directly transferred into the computer for

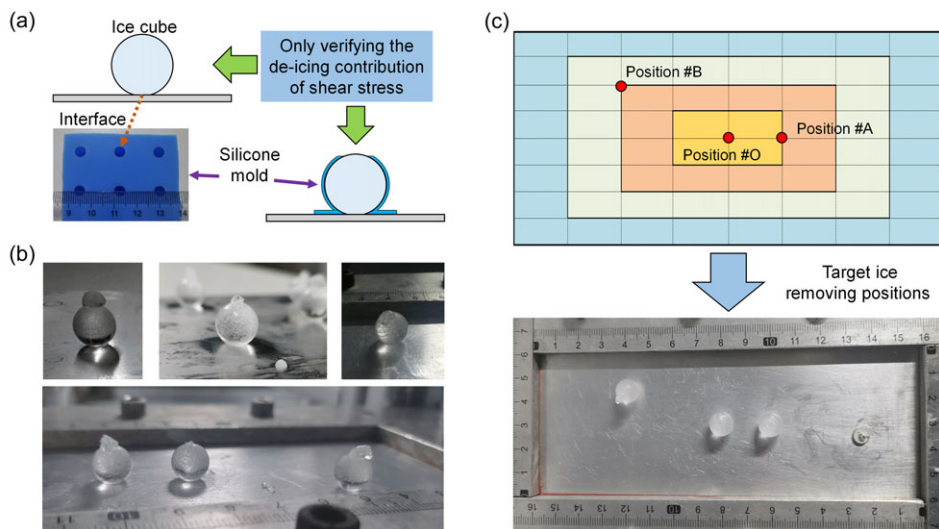


Figure 6. Indicators: (a) schematic diagram of the ice model, (b) ice-cube samples and (c) de-icing positions.

further investigation. In addition, a series matching inductor with the inductance range of 0.539 mH–12.48 mH was connected in series in the circuit during the test to be treated as an impedance matching device. The value of the series matching inductor was measured using a digital multimeter with an inductance measurement function to confirm the detailed inductance.

2.4 Icing and monitoring points settings

The shear stress is the main factor that induces the ice-removal phenomenon under the execution of the electromechanical ice protection system. However, when considering lots of experiment results and situations that were got by many researchers, the shear stress in some areas was not enough to meet de-icing requirements [20, 23]. This meant that the large-scale ice layer on the plate could not be completely removed due to some not debonded points. To fully verify the contribution that shear stress makes to de-icing and obtain obvious ice detachment phenomenon, a special ice cube type was designed instead of a sheet of ice layer to guarantee the small interface area with the substrate. For the actual inflight de-icing situation to form mixed ice or rim ice under -10°C , the supercooled droplets or ice crystals will quickly freeze on the surface of the wing, forming a small contact area with the wing [1, 2]. So the icing model set in this paper is in line with the actual inflight icing cases and also in line with the research of Zeng et al. [27]. As shown in Fig. 6a, small ice cubes that approximate spheres were used as research objects of ice to be removed.

The interface area between an ice cube and the plate has a small contact surface due to the spherical shape of the ice cubes. The formation of this ‘ice-cube sphere’ is easy to control using a spherical silicone mold with a regular, circular flat bottom to form a circular interface between the ice cube and the substrate, with a diameter of 5 mm. All the ice cubes were made in the refrigerator below about -20°C using a silicone mold and pure water. The freezing time was fixed at 10 minutes to ensure the complete freezing of the liquid water inside the silicone mold. Meanwhile, the temperature of the substrate and the ice cubes were guaranteed the same value of -20°C with the 10-minute freezing time. Some ice cubes are shown in Fig. 6b. Based on the experimental measurement data of Zeng and Rønneberg [38], the adhesive strength of ice samples on the aluminum substrate is around 0.34 MPa.

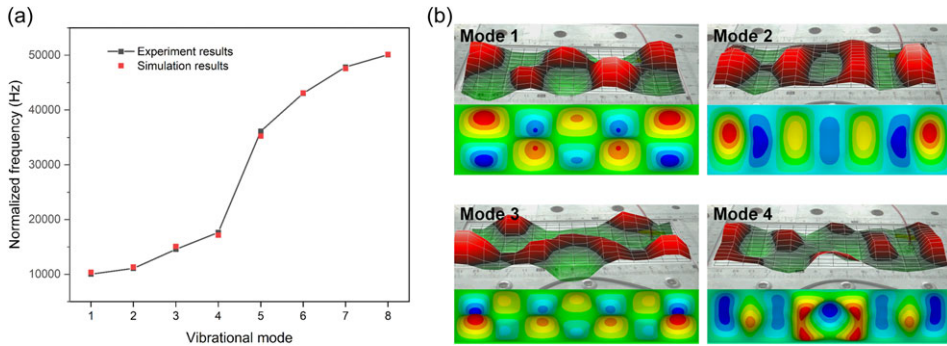


Figure 7. Comparison results: (a) frequency results and (b) various typical vibration mode shape results.

To avoid the mutual influence of different ice cubes when falling off the plate, three different small de-icing points were chosen as ice-removal areas (Fig. 6c). When synthesising the ice cubes on the plate surface, three silicone molds could be placed at a corresponding location without positional interference. Therefore, these ice cubes at three different positions for one single experiment were made at the same time in the same freezing environment.

3.0 Results and discussions

3.1 Simulation model verifications

According to the framework of the de-icing capability prediction method, simulation is the main method to determine the ISCC value for different vibrational modes. The accuracy of the adopted simulation model was verified with experimental results in this paper. Considering the features of the electromechanical structure, we divided the verifications into two perspectives: mechanical and electrical perspectives.

From the mechanical perspective, the dynamic characteristics of the whole structure excited by piezoelectric actuators were recorded. The typical vibration modes were selected according to the measurement results by a PSV-500-3D scanning laser vibrometer (Fig. 5a) to choose the frequencies of the mode shapes that can be judged. These typical vibration mode shapes and corresponding vibrational frequencies were compared. Figure 7a shows a comparison between the vibration results of the simulation and those from experimental measurement. The results show a better fit of these excitation frequencies. A comparison between the results of the simulation and those of the experiment for various typical mode shapes is shown in Fig. 7b. Moreover, the frequency range of these eight vibrational modes was 10 kHz–100 kHz, this range is also the traditional excitation frequency range used for de-icing research with resonant mechanical vibration principle in many literatures [13–16, 21, 24]. So these vibrational modes were used in this paper for different studies of the de-icing capability prediction method.

For verification from an electrical perspective, the main data for comparison were obtained by a precision-impedance analyser and simulation software. Two typical parameters of impedance and phase angle were selected to verify the simulation results using the experimental data. The results are shown in Fig. 8. The maximum percentage tolerance of phase angle is 3.4%. When considering the power factor $\cos\theta$, the tolerance of the power factor is 0.0482. The above tolerance showed good agreement between simulation and experiment.

3.2 Influence of relative parameters for ISCC determination

As discussed in section 2.1, the ISCC value is constant for a given vibrational mode. We take the simulation results at the central point of the plate (position #O) as an example to illustrate the relationships

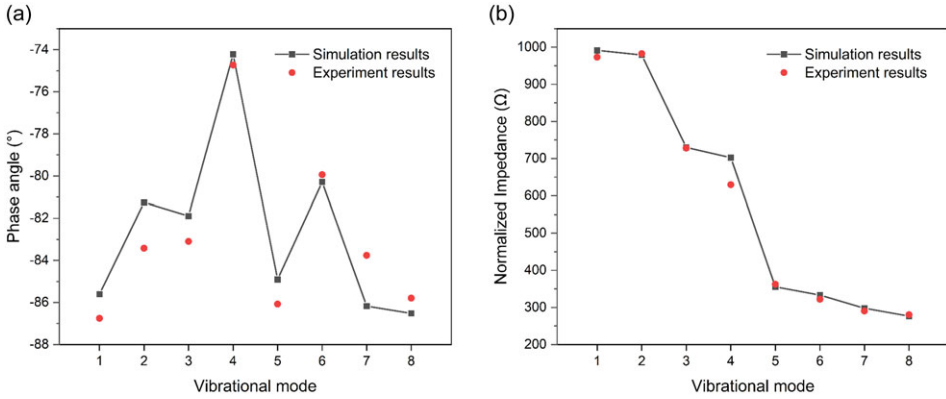


Figure 8. Comparison of electrical-parameter results: (a) phase angle results and (b) impedance results.

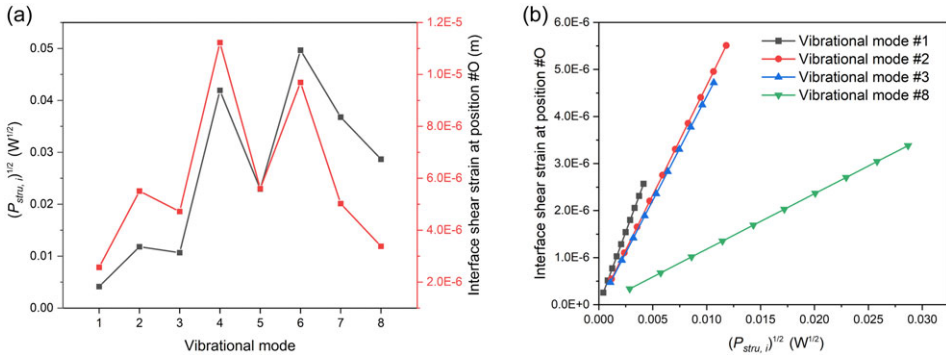


Figure 9. Relationship between interface shear strain $\gamma_{interface}$ and the square root of the whole system power $\sqrt{P_{stru,i}}$.

between interface shear stress/strain/strain and power for different vibration modes without the influence of the impedance matching effect. The relationship between interface shear strain and power was shown in Fig. 9a. And we also finished the more rigorous simulation works under different applied voltage on piezo-actuators at different vibrational frequencies. The value of applied voltage was set from 10 V to 100 V. Detail results of shear strain and mechanical power were obtained under these simulation cases. We had calculated the above results at four different vibrational modes (vibrational mode #1/2/3/8). The comparison between shear strain and mechanical power was conducted and detail result was shown in Fig. 9b. As shown in Fig. 8, the interface shear strain $\gamma_{interface}$ is proportional to the square root of the whole system power at one specific vibrational frequency $P_{stru,i}$. Meanwhile, the results also proved the conclusion summarised in section 2.1 that the ISCC value remains constant when the vibrational frequency does not change.

The numerator of ISCC (interface shear stress/strain) is a mechanical parameter, while the denominator of ISCC (power) will have different types in mechanical or electrical aspects. The interface shear stress/strain is the unique parameter, while the power parameter has different forms. From the simulation point of view, the power related to the interface shear stress/strain will have the following categories: mechanical vibration power $P_{stru,i}$ and simulation electrical power P_e . From an experimental point of view, the system power P_{exp} will be the actual load power transferred from the excitation source to piezoelectric

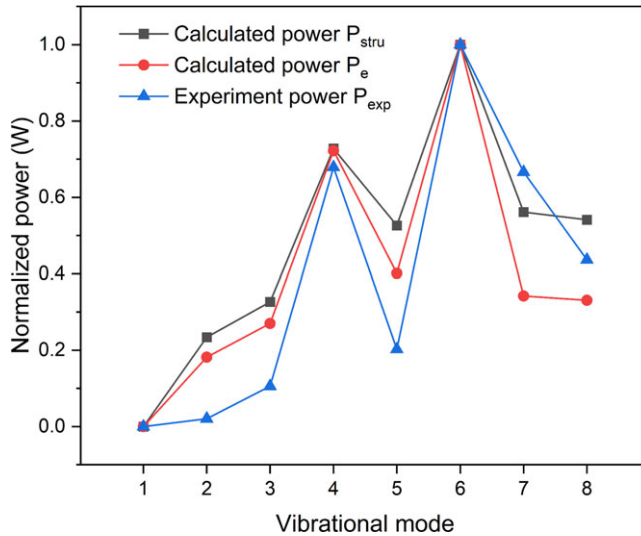


Figure 10. Different power parameters comparison results.

actuators for ice removal. Figure 10 shows a comparison of the results for these different power parameters without integrating any impedance-matching devices. These three power parameters have similar distribution laws. This result shows the agreement between the simulation data and the experimental data in terms of power parameters. Considering the types of different power parameters, the mechanical power parameter ($P_{stru,i}$) is consistent with the electrical power parameters (P_e and P_{exp}). Based on the operating principle of piezoelectric actuators, the input electrical excitation power can be converted into the mechanical vibration power. Therefore, these power parameters are equivalent in the calculation of the ISCC. According to the description in section 2.1, the calculation of ISCC by simulation method can be carried out with different simulation power parameters. The premise of this calculation method to determine ISCC is to ensure that the same power parameters are used for each vibrational mode.

3.3 Influence of impedance matching effect on mechanical vibration

The important role of energy and power in de-icing has been discussed previously [37, 39]. Sufficient load power is the basis for ensuring the de-icing effect. For an EDS, the load power is controlled by the system impedance and the power factors. Due to the existence of impedance, the sufficient load power applied onto the piezo-actuator only occupies a part of the whole output power. Therefore, impedance-matching attempts to improve the effective load power required to boost the piezoelectric actuators at a determined applied voltage. Measurement impedance results of a de-icing system with a series-matching inductor are shown in Fig. 11a. The presence of a series matching inductor reduces the inductance and capacitance components in the equivalent circuit of the EDS. As a result, the electrical impedance value of the overall system is significantly reduced, especially for a high frequency vibrational mode. Meanwhile, the impedance matching effect of the series inductor improves power-factor levels (Fig. 11b) due to the adjustment of the phase angle of the current vector and voltage vector. This means that the equivalent circuit is close to a pure resistance circuit if the appropriate impedance-matching device is added. Without considering the resistance adjustment between the equivalent circuit and excitation source, the impedance matching effect can increase the effective output power of the overall de-icing system. So, according to Equations (4) and (5), the final excitation force F_{stru} will be improved due to the increasing electromechanical coupling coefficient. This also results in the effective output power enhancement in the de-icing system.

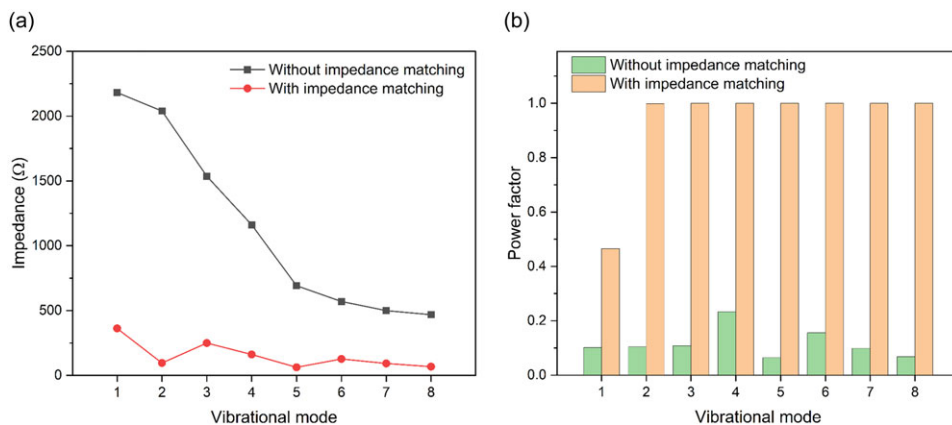


Figure 11. Variation results of impedance and power factor before and after impedance matching.

Now move to the discussion about the mechanical vibration of the system under the impact of the impedance matching effect. In section 2.1 we assumed that the existence of a series-matching inductor doesn't affect the mechanical characteristics of the system due to its electric features. Some experiments were carried out to check whether the assumption was right. Two different vibrational modes were selected in the experiment. The experiment setups described in Fig. 5a and 5b were used to test the influence of impedance impedance-matching effect on the final structural mechanical vibration. The series-matching inductor was adjusted with different values to change the final series inductance of the system, and corresponding peak vibrational displacements at various load powers were measured. Detail displacement results are shown in Fig. 12a. The relative mean value and square deviation are displayed in Fig. 12b. This leads to the conclusion that the structural vibration displacement remains constant for the same power, regardless of the actual system inductance. From another point of view, the change in impedance matching effect does not affect the mechanical vibration of the structure under the same load power conditions. So the results verify the correctness of the assumption presented in section 2.1. Meanwhile, the de-icing capability prediction method proposed in this paper based on this assumption is also verified. So the ISCC value will not change under the existence of a series-matching inductor. The calculated ISCC with the simulation method without the impact of the impedance matching effect can be used in Equation (7) to determine the actual interface shear stress/strain values.

Based on the expression in Equation (7) and the results in Fig. 11, the improved power by adding an appropriate series-matching inductor will increase the interface shear stress/strain values for the de-icing application. E.g., for vibration mode 8, when the series-matching inductor is added into the system, the interface shear stress/strain is about 10.12 times higher than the original system without impedance-matching component under constant voltage applied on piezoelectric actuators. This is also the significance of the impedance matching effect for the improvement of de-icing capability.

3.4 Actual de-icing cases for de-icing capability prediction method verification

According to the de-icing capability prediction procedure summarised in section 2.1, the detailed de-icing performance of the de-icing structure under eight vibrational modes was evaluated under the existence of an impedance impedance-matching device. Figure 13 shows the simulation results of the ISCC values with different vibrational modes on various positions. Relative locations of these three de-icing positions are shown in Fig. 6c. It can be found from Fig. 13a that vibration modes at lower frequency regions have higher ISCC values than the corresponding values of the vibration modes at higher frequency areas. So if the same load power is applied to the piezoelectric actuators, the vibration modes

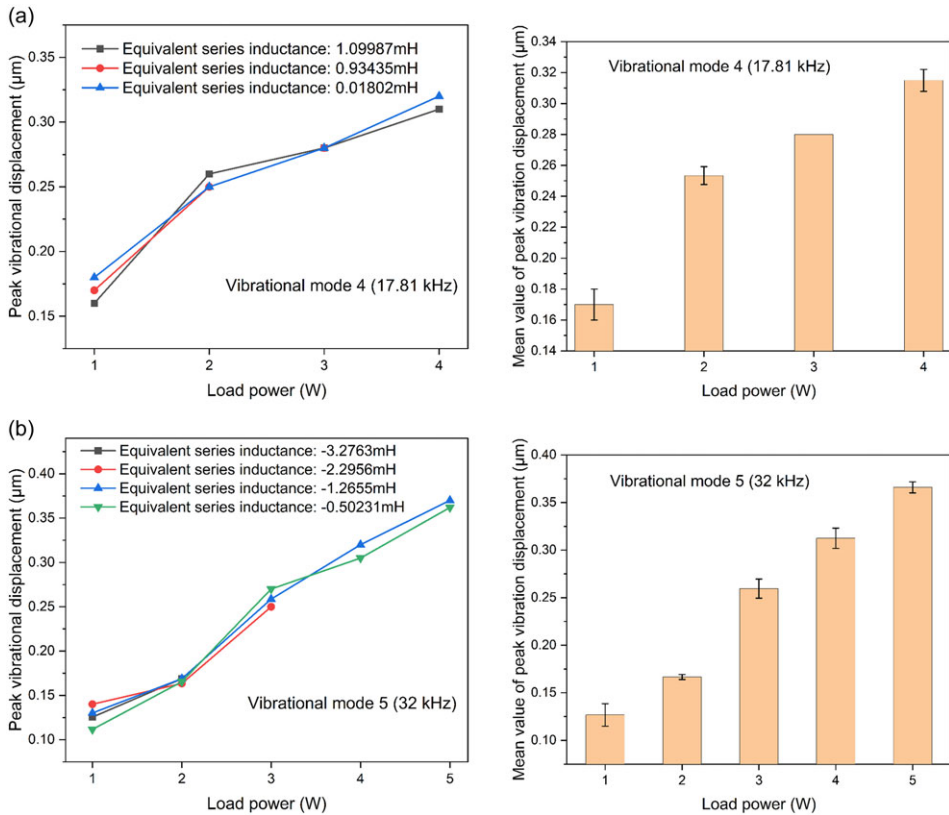


Figure 12. Peak vibrational displacements at various load powers and system series inductance.

with higher ISCC values will exhibit a stronger de-icing capability due to the higher interface shear stress/strain for inducing ice layer delamination.

As shown in Fig. 13b, in comparison with the three positions, position #A is in the place where the displacement gradient changes drastically, so it has a greater shear stress than other positions under the same load energy. The displacement gradient of the position of #O and #B is different in the case of vibrational mode 1, this leads to the different interface shear stress of these two positions. Considering the displacement gradient of position #B and #O in other vibrational modes, one can find that the gradients are similar, so they have similar shear stress. It can be concluded from Fig. 13 that the position where the displacement gradient changes drastically has a larger interface shear stress, so it has a larger ISCC value.

The second result to be discussed was the actual load powers measurement by experiment equipment. The actual pre-excitation vibration testing setup is shown in Fig. 5c. The testing sample was placed into the refrigerator to guarantee the same cold environment as the following de-icing test. The actual power of the de-icing system at different vibration frequencies was measured by a power amplifier under the impact of impedance matching device and is shown in Fig. 14. The results show that the actual power in the low-frequency range is less than the power in high-frequency range due to the large equivalent series inductance. Although the presence of a series inductor can reduce the equivalent series inductance of the entire circuit, the equivalent impedance achieved by the impedance matching method is still large due to the large value of the original inductance. However, for the high-frequency case where the original inductance is small, the impact of the impedance matching method is more obvious. This is the reason why the final real power is higher in the high-frequency cases. This is also the reason why

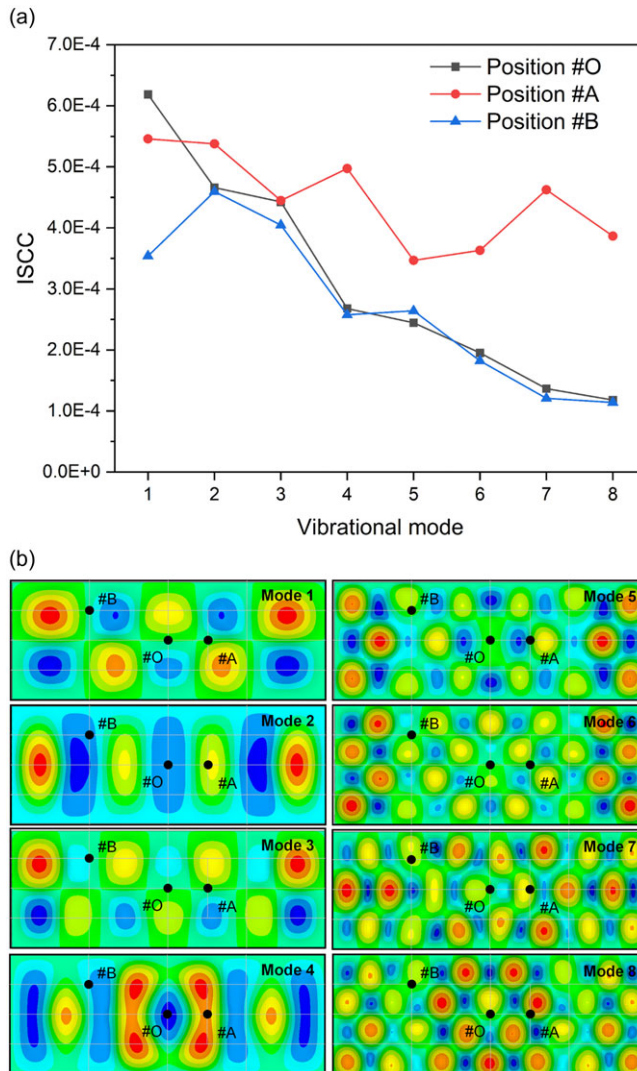


Figure 13. Calculation results of ISCC without impedance-matching device at different positions.

many studies on electromechanical de-icing tend to choose high-frequency excitation and rarely choose low-frequency excitation [14, 15, 26–28].

The predicted interface shear stress/strain at different positions on the plate were calculated according to the expression in Equation (7), the results are shown in Fig. 15. It can be found in the figure that vibration modes in the high-frequency range (mode 4–8) will exhibit better de-icing capability due to the high interface shear strain/stress under the impact of impedance matching device. Meanwhile, vibration mode 1 and mode 3 will show poor de-icing performance due to the smaller interface shear stress/strain. And from the power point of view, the actual powers in mode 4–8 have a higher level than the powers in mode 1–3. Based on the previous studies by many scholars on the electromechanical de-icing method with high excitation power [16, 33], the ice delamination phenomenon in mode 4–8 will be easily obtained due to the large interface shear stress/strain and enough power supply from the excitation source.

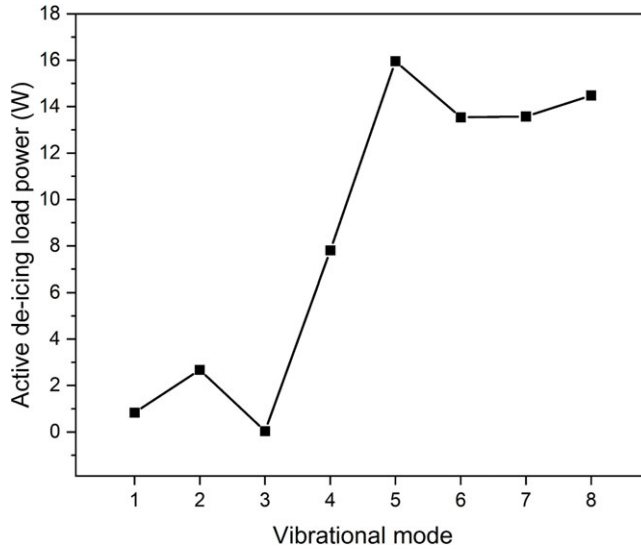


Figure 14. Actual power of the de-icing system at different vibration frequencies.

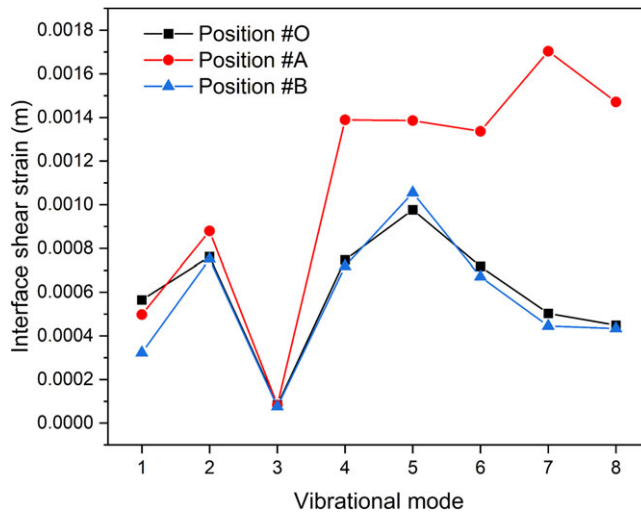
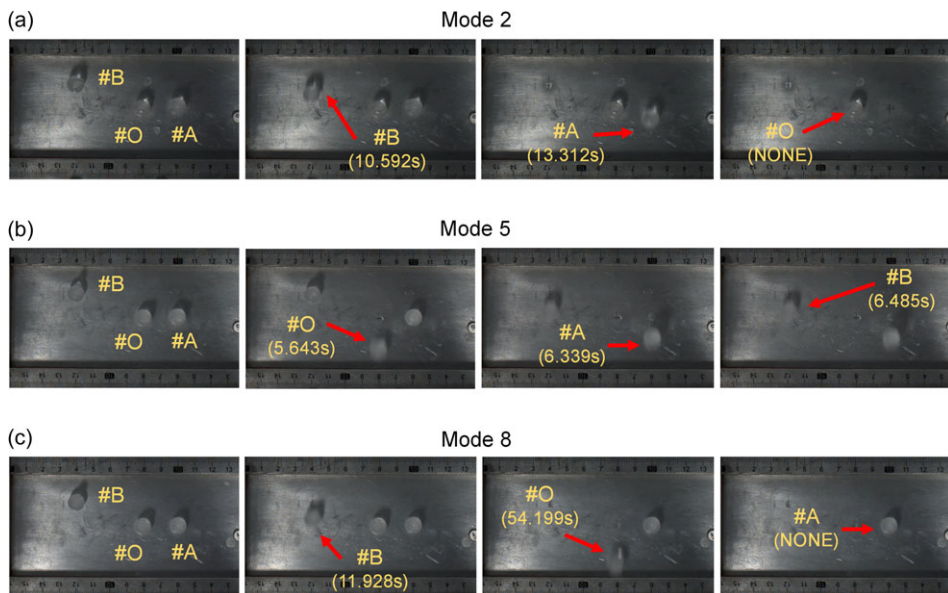


Figure 15. Actual interface shear strain at different positions with impedance-matching components.

With the calculated interface shear stress/strain of each vibration mode under the actual load power of the system, relative ice removal experiments were carried out to confirm the actual de-icing capability of these vibrational modes. Detail tests for de-icing were implemented with the experiment setup described in Fig. 5c. And all the de-icing tests were conducted in the refrigerator below about -20°C , which was the same temperature for ice cube manufacture. De-icing tests for each mode were carried out three times to guarantee the repeatability of the experiments. According to the de-icing results for different vibrational modes, the positions with the ice delamination phenomenon were consistent in the three repeated experiments. Combining all the results of de-icing time, the maximum standard deviation of de-icing time in repeated experiments was 0.67545. This result proves the repeatability of the experimental results. The experiment results are listed in Table 2, and some typical ice-removal results are shown in Fig. 16.

Table 2. Summary of de-icing experiment results

Vibration mode no.	De-icing frequency, kHz	Excitation voltage, V_{p-p}	Excitation current, A_{p-p}	De-icing results		
				Position #O	Position #A	Position #B
Mode 1	10.030	140	0.20	Failure	Failure	Success
Mode 2	11.085	140	0.16	Failure	Success	Success
Mode 3	14.550	140	0.04	Failure	Failure	Failure
Mode 4	17.810	140	0.50	Success	Success	Success
Mode 5	32.000	100	1.38	Success	Success	Success
Mode 6	43.800	100	1.00	Success	Success	Success
Mode 7	48.000	100	1.12	Success	Success	Success
Mode 8	51.100	60	1.90	Success	Failure	Success

**Figure 16.** Typical ice-removal experiment results: (a) mode 2, (b) mode 5 and (c) mode 8.

The relationship between ice-removal time and actual predicted interface shear stress/strain at different positions is shown in Fig. 17. The results show that the actual predicted interface shear/strain after impedance matching is inversely proportional to the de-icing time at three different positions. On the other hand, vibration modes and positions with a large, predicted interface shear/strain will lead to greater de-icing capability. The de-icing capability prediction method introduced in this paper was verified by experiment results and proved its feasibility in the actual de-icing process.

Moreover, the prediction method considering the impact of impedance matching devices also can be used for the selection of potential de-icing modes. On the premise that the de-icing position is known, the vibrational mode with larger interface shear stress/strain appears at this position, which has better de-icing capability. Therefore, when evaluating whether the actual vibration mode is suitable for de-icing applications, the interface shear stress/strain corresponding to the actual experimental load power can be achieved by the prediction method presented in this paper. Based on Equation (7), the load power is the fundament for the generation of interface shear stress/strain. So if the de-icing system can obtain large load power for de-icing purposes under one specific vibration mode with an impedance matching device,

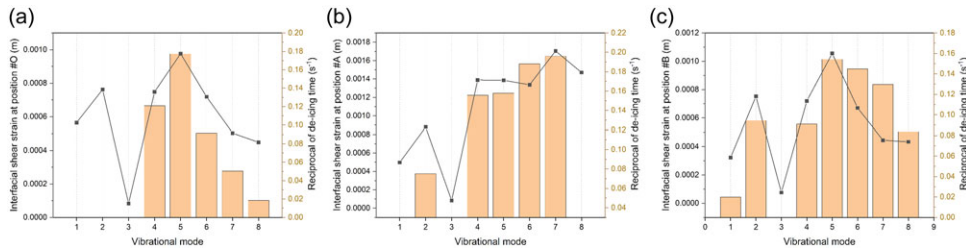


Figure 17. Relationships between ice-removal time (experiment) and interface shear strain (simulation) at different de-icing positions: (a) results at position #O, (b) results at position #A and (c) results at position #B.

ice delamination will easily be achieved due to the large actual interface shear stress/strain. That's also the reason that many scholars choose ultrasonic frequencies to carry out their ice protection research due to the higher load power gained from excitation sources in ultrasonic frequency ranges.

The actual applied voltage of each vibration mode is also shown in Table 2. The real output power of the piezoelectric actuators is determined by the electrical characteristics of the corresponding electromechanical system for different vibration modes. For a vibration mode with a better electromechanical conversion efficiency and a higher power factor, a higher output power is obtained from the piezoelectric actuators at a constant applied voltage due to the lower impedance value. Meanwhile, a lower applied voltage can also excite enough output power on the actuators for ice-removal due to the lower impedance value (e.g., the actual experiment power of mode 5–8 under 100V&60V is higher than mode 1–4 due to the better electromechanical conversion efficiency). This enough output power in turn leads to greater de-icing interface shear forces. In other words, this means that low-voltage-driven de-icing targets can be achieved with these vibration modes if the impedance matching method can guarantee a higher power factor of the de-icing system. This can also be predicted by the de-icing capability prediction method considering the impact of the impedance matching device by using simulation results and measurement data. Finally, when considering the power consumption level in the de-icing experiment, the maximum power consumption per unit area in all modal de-icing experiments is 0.167 W/cm^2 , which is smaller than the de-icing energy consumption (0.95 W/cm^2) of the electric heating system described in the literature [4].

4.0 Conclusions

In this paper, the de-icing capability prediction method of the EDS with the impact of the impedance matching effect was proposed. The main goal of the current study was to analyse the actual de-icing performance according to the interface shear stress/strain with different vibration modes. An impedance-matching device was added to the system to improve the output power for de-icing purposes. The main conclusions are summarised as follows:

A de-icing capability prediction method considering the impedance matching effect was introduced in this paper. The prediction method was proposed based on both simulation results and experiment results. The application procedure of this proposed method was summarised and verified in this paper for actual application.

The simulation model without considering the impedance matching effect was verified with experiment results. The mechanical vibration frequencies and mode shapes had a good matching result in the simulation and experiment aspects. Meanwhile, the simulated electrical parameters (impedance and phase angle) also had good agreement with the experimental results.

The impedance-matching method with a series-matching inductor is found to improve the electrical characteristics of the whole de-icing system, without affecting the structural mechanical vibration. It

is indicated that the value of ISCC is not affected by the existence of a series-matching inductor. The simulated ISCC without the impedance matching effect is adopted to determine the actual interface shear stress/strain values in the cases with impedance matching devices.

The feasibility of the proposed de-icing capability prediction method considering the impedance matching effect was verified its feasibility with actual de-icing cases. The actual interface shear stress/strain of the structure for different vibration modes was inversely proportional to the actual de-icing time. The vibration mode with high actual interface shear stress/strain at the target position will be selected as the de-icing mode, due to its high de-icing capability. This operation can also be performed by the de-icing capability prediction method established in this paper. In addition, low-voltage-controlled de-icing targets have been achieved and predicted by this method when the impedance matching effect can guarantee a higher power factor of the de-icing system.

The paper examines a de-icing capability prediction method utilised by a system integrated with an impedance-matching device. The focus is on a pre-existing de-icing structure that has been bonded with piezoelectric actuators. The initial design of EDS is to study the dynamic characteristics of substrate structure (such as the aircraft wing skin structure) and trying to obtain the basic structure vibrational mode for the arrangement design of piezoelectric actuators. So there is a need to expand the application of this method to structures before bonding piezoelectric ceramics, and coupling this method into the process of initial basic structure vibrational mode selection. Meanwhile, the future research also needs to be focused on the application of this prediction method under different icing conditions, as well as on the rapid prediction results processing technology development with the changing state in EDS characteristics due to changing flight environments.

Acknowledgements. This work was funded by the National Natural Science Foundation of China (Grant No. 11832012, 12227802) and the Fundamental Research Funds for the Central Universities (Grant No. 3082020NP2020402). The authors gratefully acknowledge the support of the State Key Laboratory of Mechanics and Control of Mechanical Structures, many of the vibration mode measurements presented in this paper were performed in this lab.

Competing interests. The author(s) declare that they have no competing interests.

References

- [1] Tetteh E., Loth E., Neuteboom M.O. and Fisher J. In-flight gas turbine engine icing. *AIAA J.*, 2022, **60**, (10), pp 5610–5632.
- [2] Bromfield M.A., Horri N., Halvorsen K. and Lande K. Loss of control in flight accident case study: icing-related Tailplane stall. *Aeronaut. J.*, 2023, **127**, (1315), pp 1554–1573.
- [3] Chen N., Hu Y., Ji H. and Zhang M. Hot-air anti-icing heat transfer and surface temperature modeling. *AIAA J.*, 2021, **59**, (9), pp 3657–3666.
- [4] Yang S., Yi X., Guo Q., Xiao C., Luo Z. and Zhou Y. Novel hybrid ice protection system combining thermoelectric system and synthetic jet actuator. *AIAA J.*, 2021, **59**, (4), pp 1496–1500.
- [5] Koivisto P., Honkanen T., Auvinen M., Hellsten A. and Kahma K. De-icing fluid flow-off from a flat plate in an accelerating airstream. *AIAA J.*, 2020, **58**, (4), pp 1607–1619.
- [6] Hu H., Meng X., Cai J., Zhou W., Liu Y. and Hu H. Optimization of dielectric barrier discharge plasma actuators for icing control. *J. Aircraft*, 2020, **57**, (2), pp 383–387.
- [7] Han N., Hu H. and Hu H. An experimental investigation to assess the effectiveness of various anti-icing coatings for UAV propeller icing mitigation. *AIAA AVIATION 2022 Forum*, Chicago, IL & Virtual Event, 2022.
- [8] Burch J.D., Han D. and Averkin S.N. Numerical investigations of 2-D planar magnetic nozzle effects on pulsed plasma plumes. *Aeronaut. J.*, 2022, **126**, (1299), pp 793–812.
- [9] Li D.W., Lin M.X. and Tian L. Research and modeling of force fighting equalisation for aircraft rudder's triple active actuation system. *Aeronaut. J.*, 2022, **126**, (1304), pp 1801–1814.
- [10] Adachi K., Saiki K. and Sato H. Suppression of frosting on a metal surface using ultrasonic vibrations. *1998 IEEE Ultrason. Symp. Proc.*, Sendai, Japan, 1998.
- [11] DiPlacido N., Soltis J. and Palacios J. Enhancement of ultrasonic de-icing via tone burst excitation. *J. Aircraft*, 2016, **53**, (6), pp 1821–1829.
- [12] Kalkowski M.K., Rustighi E. and Waters T.P. Modelling piezoelectric excitation in waveguides using the semi-analytical finite element method. *Comput. Struct.*, 2016, **173**, pp 174–186.
- [13] Venna S.V., Lin Y.J. and Botura G. Piezoelectric transducer actuated leading edge de-icing with simultaneous shear and impulse forces. *J. Aircraft*, 2007, **44**, (2), pp 509–515.
- [14] Palacios J., Smith E., Rose J. and Royer R. Ultrasonic de-icing of wind-tunnel impact icing. *J. Aircraft*, 2011, **48**, (3), pp 1020–1027.

- [15] Palacios J., Smith E., Rose J. and Royer R. Instantaneous de-icing of freezer ice via ultrasonic actuation. *AIAA J.*, 2011, **49**, (6), pp 1158–1167.
- [16] Budinger M., Pommier-Budinger V., Napias G. and Costa da Silva A. Ultrasonic ice protection systems: analytical and numerical models for architecture tradeoff. *J. Aircraft*, 2016, **53**, (3), pp 680–690.
- [17] Guo F. and Wu J.H. Analytical solution and coupling resonance mechanism of interface delamination of composite laminates excited by ultrasonic shear horizontal waves. *Compos. Struct.*, 2021, **276**, p 114583.
- [18] Guo F. and Wu J.H. Coupling resonance mechanism of interfacial fatigue stratification of adhesive and/or welding butt joint structures excited by horizontal shear waves. *Int. J. Mod. Phys. B*, 2021, **35**, (7), p 2150096.
- [19] Guo F. and Wu J.H. Mechanism and prediction models for interfacial shear separation of claddings excited by Love waves. *Adv. Mech. Eng.*, 2021, **13**, (3), p 16878140211005196.
- [20] Wang Y., Xu Y. and Lei Y. An effect assessment and prediction method of ultrasonic de-icing for composite wind turbine blades. *Renew. Energy*, 2018, **118**, pp 1015–1023.
- [21] Daniliuk V., Xu Y., Liu R., He T. and Wang X. Ultrasonic de-icing of wind turbine blades: performance comparison of perspective transducers. *Renew. Energy*, 2020, **145**, pp 2005–2018.
- [22] Wang Z., Xu Y. and Gu Y. A light lithium niobate transducer design and ultrasonic de-icing research for aircraft wing. *Energy*, 2015, **87**, pp 173–181.
- [23] Shi Y. and Jia Y. Multimodal shear wave de-icing using fiber piezoelectric actuator on composite for aircraft wings. *IEEE-ASME T. Mech.*, 2018, **23**, (5), pp 2090–2098.
- [24] Overmeyer A., Palacios J. and Smith E. Ultrasonic de-icing bondline design and rotor ice testing. *AIAA J.*, 2013, **51**, (12), pp 2965–2976.
- [25] Miao B., Li W., Yuan L. and Zhu C. Determining region of installation of flat-ended piezoelectric de-icing actuators on curved surfaces. *J. Aircraft*, 2023, **60**, (1), pp 232–244.
- [26] Strobl T., Storm S., Thompson D., Hornung M. and Thielecke F. Feasibility study of a hybrid ice protection system. *J. Aircraft*, 2015, **52**, (6), pp 2064–2076.
- [27] Zeng X., Yan Z., Lu Y., Fu Y., Lv X., Yuan W. and He Y. Reduction of ice adhesion using surface acoustic waves: nanoscale vibration and interface heating effects. *Langmuir*, 2021, **37**, (40), pp 11851–11858.
- [28] Garcia J., Huré M., Olivier P., Budinger M. and Tepylo N. Numerical simulation of ice shedding from an icephobic surface using a four-point bending test and cohesive zone modeling. Available at SSRN 4092186.
- [29] Lin S. and Xu J. Effect of the matching circuit on the electromechanical characteristics of sandwiched piezoelectric transducers. *Sensors*, 2017, **17**, (2), p 329.
- [30] Rathod V.T. A review of acoustic impedance matching techniques for piezoelectric sensors and transducers. *Sensors*, 2020, **20**, (14), p 4051.
- [31] Yao M., Li J. and Niu Y. Adaptive impedance matching for power management circuit for a piezoelectric energy harvester on the bridge. *Sensor Actuat. A-Phys.*, 2021, **331**, p 112986.
- [32] Maio L., Piscitelli F., Ameduri S., et al., On the use of smart on-board systems for aircraft ice removal. *2020 IEEE 7th Int. Workshop Metrol. AeroSp. (MetroAeroSp.)*, Pisa, Italy, 2020.
- [33] Budinger M., Pommier-Budinger V., Bennani L., Rousset P., Bonaccorso E. and Dezitter F. Electromechanical resonant ice protection systems: analysis of fracture propagation mechanisms. *AIAA J.*, 2018, **56**, (11), pp 4412–4422.
- [34] Villeneuve E., Ghinet S. and Volat C. Experimental study of a Piezoelectric de-icing system implemented to rotorcraft blades. *Appl. Sci.*, 2021, **11**, (21), p 9869.
- [35] Maio L., Piscopo R. and Ricci F. An adaptive impedance matching network for ultrasonic de-icing. *Eur. Workshop Struct. Health Monit.*, 2022, **3**, pp 806–811.
- [36] Wang H. and Qin Q.H. *Methods of Fundamental Solutions in Solid Mechanics*. Cambridge: Elsevier, 2019.
- [37] Budinger M., Pommier-Budinger V., Reyssat A. and Palanque V. Electromechanical resonant ice protection systems: energetic and power considerations. *AIAA J.*, 2021, **59**, (7), pp 2590–2602.
- [38] Rønneberg S., Zhuo Y., Laforte C., He J. and Zhang Z. Interlaboratory study of ice adhesion using different techniques. *Coatings*, 2019, **9**, (10), p 678.
- [39] Shi Z., Kang Z., Xie Q., Tian Y., Zhao Y. and Zhang J. Ultrasonic deicing efficiency prediction and validation for a flat deicing system. *Appl. Sci.*, 2020, **10**, (19), p 6640.